Nanomanufacturing and Metrology (2023) 6:2
https://doi.org/10.1007/s41871-023-00183-9

ORIGINAL ARTICLE

Facile and Economical Fabrication of Superhydrophobic Flexible Resistive Strain Sensors for Human Motion Detection

Yulin Shang[1] · Bingzhen Zhang[1] · Jiyu Liu[1] · Chunwen Xia[1] · Xiaowei Yang[1] · Defeng Yan[1] · Jing Sun[1]

Received: 6 October 2022 / Revised: 21 December 2022 / Accepted: 4 January 2023

Abstract

Superhydrophobic flexible strain sensors have great application value in the fields of personal health monitoring, human motion detection, and soft robotics due to their good flexibility and high sensitivity. However, complicated preparation processes and costly processing procedures have limited their development. To overcome these limitations, in this work we develop a facile and low-cost method for fabricating superhydrophobic flexible strain sensor via spraying carbon black (CB) nanoparticles dispersed in a thermoplastic elastomer (SEBS) solution on a polydimethylsiloxane (PDMS) flexible substrate. The prepared strain sensor had a large water contact angle of $153 \pm 2.83°$ and a small rolling angle of $8.5 \pm 1.04°$, and exhibited excellent self-cleaning property. Due to the excellent superhydrophobicity, aqueous acid, salt, and alkali could quickly roll off the flexible strain sensor. In addition, the sensor showed excellent sensitivity (gauge factor (GF) of 5.4–7.35), wide sensing ranges (stretching: over 70%), good linearity (three linear regions), low hysteresis (hysteresis error of 4.8%), and a stable response over 100 stretching-releasing cycles. Moreover, the sensor was also capable of effectively detecting human motion signals like finger bending and wrist bending, showing promising application prospects in wearable electronic devices, personalized health monitoring, etc.

Article Highlights

1. The process of preparing of the CB-SEBS/PDMS superhydrophobic flexible strain sensor is proposed.
2. The relationship between the superhydrophobicity of the conductive coating and the mass percentage of the SEBS is analyzed.
3. The properties and promising applications of the CB-SEBS/PDMS sensor are discussed.

Keywords Superhydrophobic · Spraying · Strain sensors · Human motion detection

1 Introduction

Thanks to its high flexibility and good sensitivity, a flexible strain sensor has promising application prospects in the fields of personal health monitoring, human motion detection, human–machine interfaces, and soft robotics [1–3]. Compared to rigid metal strain sensors and semiconductor strain sensors, the flexible strain sensor is more suitable for wearable electronic devices due to their good flexibility, light weight, and easy recovery from deformation [4–6]. However, during practical applications, the flexible strain sensor is susceptible to humid, acidic, and alkaline environments, which may result in invalidation of the sensor.

✉ Defeng Yan
yandefeng1994@163.com

✉ Jing Sun
sunjing@dlut.edu.cn

[1] Key Laboratory for Precision and Non-Traditional Machining Technology of the Ministry of Education, Dalian University of Technology, Dalian 116024, People's Republic of China

Published online: 03 March 2023

In nature, lotus leaves are born in the dirt but remain unstained, which attracts the interest of researchers [7]. They have discovered that the self-cleaning ability is attributed to the superhydrophobic property of the lotus leaves [8–10]. A superhydrophobic surface usually refers to a surface with a large water contact angle (CA > 150°) [11, 12]. In addition, water droplets can easily roll off the superhydrophobic surface with a tilted angle of less than 10° [13, 14]. Thus, the superhydrophobic surface can protect the sensor from being wetted by liquids like acids, bases and salts, thereby ensuring the sensor to operate under humid and corrosive conditions with high performance [15]. To date, a lot of research has been conducted to apply the superhydrophobic surface in the flexible strain sensor [16–28]. Liu et al. prepared a multifunctional silicone rubber/multi-walled carbon nanotubes/laser-induced graphene/silicone rubber (SR/MWCNTs/LI- G/SR) superhydrophobic composite strain sensor by integrating a MWCNTs/LIG cross-linked conductive network layer, a superhydrophobic layer, and a stretchable SR layer in a sandwich sensor via laser direct writing [17]. Ding et al. fabricated superhydrophobic flexible conductive thermoplastic elastomer/carbon nanotube (TPE/CNTs) films with higher sensing performance, exploiting the phase separation at the air–water interface. The film could operate as a sensor to detect various human motions even under high mechanical deformation and harsh environments [20]. Gao et al. decorated SiO_2 nanoparticles/graphene onto polyurethanes (PU) nanofiber prepared by the electrospinning to obtain superhydrophobic strain sensors with high sensitivity and excellent durability [23]. Li et al. prepared multifunctional smart coatings through spraying multi-walled carbon nanotubes dispersed in a thermoplastic elastomer solution, followed by ethanol treatment. The superhydrophobic conductive coatings could be prepared on different substrates and applied to full-range and real-time detection of human motion, while showing extreme repellency of water, acid, and alkali [28]. These works provided enlightenment for preparing high-performance sensors for use in harsh environments. Nevertheless, the preparation processes were generally time-consuming, and tended to involve high-cost methods, such as laser direct writing, transferring, and electrospinning. Hence, it remains challenging to prepare the superhydrophobic strain sensor with good flexibility and sensitivity using a simple and economical method.

In this work, we proposed a facile and high-efficient method to fabricate a superhydrophobic flexible strain sensor via spraying carbon black (CB) nanoparticles dispersed in a thermoplastic elastomer (SEBS) solution on a polydimethylsiloxane (PDMS) flexible substrate. The prepared strain sensor exhibited good superhydrophobicity and showed excellent repellency in corrosive environments such as acids and alkalis. Meanwhile, the sensor could be used for precise detection of various human motions. The prepared CB-SEBS/PDMS superhydrophobic flexible strain sensor is expected to have promising application prospects in various harsh environments.

2 Experimental

2.1 Materials

PDMS (Sylgard 184) base and curing agent were purchased from Dow Corning. CB nanoparticles with an average particle size of 10 nm were provided by Shanghai Maclean Biochemical Science and Technology Co. Ltd. SEBS powder was purchased from TSRC (Nantong) Industrial Co. Ltd. Cyclohexane (analytical purity) was provided by Guangdong Guanghua Technology Co. Ltd. Hydrochloric acid (HCl), sodium chloride (NaCl), and sodium hydroxide (NaOH) were purchased from Dalian Bono Chemical Reagent Co. Ltd.

2.2 Experimental Preparation

Figure 1 illustrates the processes of preparing the CB-SEBS/PDMS superhydrophobic flexible strain sensor. First, PDMS base and curing agent were uniformly mixed in the ratio of 10:1, followed by vacuum de-bubbling for 10 min. Afterwards, the mixture was spin-coated onto a plastic Petri dish and cured in an oven (101-3AB, Tianjin Taisite Instrument Co. Ltd) at 60 °C for 3 h [29], and the superhydrophobic conductive coating was then obtained. The CB nanoparticles were dispersed into 80 ml of cyclohexane by ultrasonic treatment using an ultrasonic cleaner (JP-020, Skymen Cleaning Equipment Shenzhen Eidelberg Instruments Ltd.) for 1 h, followed by magnetic stirring for 1 h to fully dissolve the SEBS powder, resulting in a homogeneous ink solution.

Fig. 1 Schematic diagram of the preparation processes of the CB-SEBS/PDMS superhydrophobic flexible strain sensor

Finally, the ink solution was applied to the prepared PDMS substrate via the spraying-coating method [28, 30]. The spraying pressure was kept at 40 psi. The distance between the spray gun and the substrate was about 15 cm, and the spraying speed was about 2 cm/ s. Due to the nano-scale CB particles and the SEBS with good flexibility and viscosity in the ink solution, a superhydrophobic and conductive coating was constructed on the PDMS substrate surface, which could be used for strain detection.

2.3 Characterization

The morphology of the samples was characterized by a scanning electron microscope (SEM, JSM-6360LV, Japan). The element compositions were characterized by an energy dispersive spectroscope (EDS, JSM-6360LV, Japan). The water contact angle (CA) and rolling angle (RA) of the sample surface were measured immediately after dropping water droplet with the volumes of 5 µl and 10 µl under room temperature, respectively, by an optical CA measuring device (SL200KS, USA). The average water CA and RA for the same sample were obtained by measuring at five different positions on the sample [31]. The tensile properties of the strain transducers were tested at room temperature using a tensile tester (HPH, Eidelberg Instruments Co. Ltd.), and the changes in resistance were recorded simultaneously using a benchtop digital multimeter (XDM1041, Fujian Lilliput Optoelectronics Technology Co. Ltd).

3 Results and Discussion

3.1 Superhydrophobicity of Flexible Strain Sensor

Due to its good flexibility, the PDMS could endow the strain sensor with excellent tensile strength and flexibility; while the CB nanoparticle coating facilitated the construction of a conductive network, so that the sensor had good conductivity. However, the coating could not be firmly adhered to the PDMS substrate relying only on the adhesion of the PDMS.

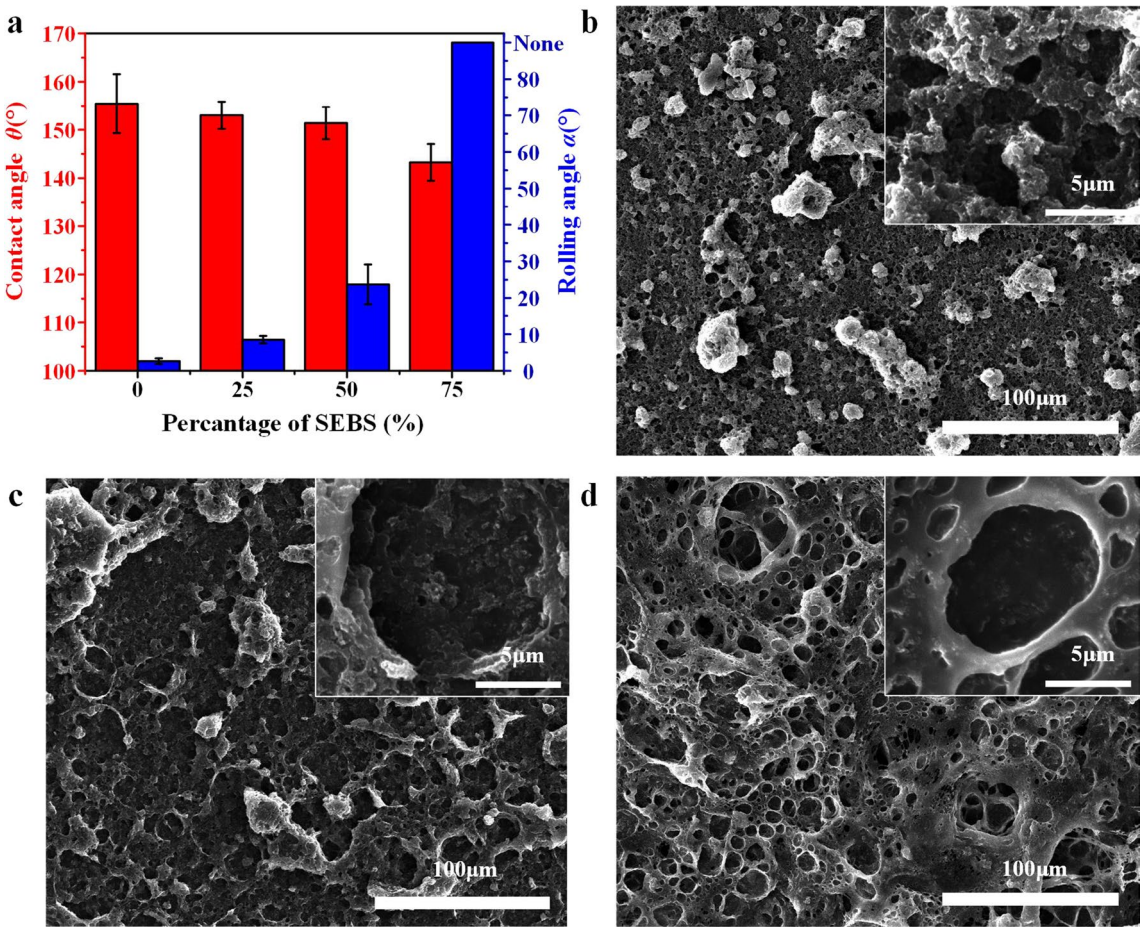

Fig. 2 **a** Contact angle and rolling angle of the sample surface at different addition ratios of the SEBS, **b** SEM image of the sample surface with 25% addition ratio of the SEBS, **c** SEM image of the sample surface with 50% addition ratio of the SEBS, **d** SEM image of the sample surface with 75% addition ratio of the SEBS

In the absence of binding agents, the contact angle was large and the rolling angle was small; however, the CB nanoparticles were only loosely adhered to the PDMS substrate, and this bond was not secure enough. Therefore, we chose to add the SEBS to improve the binding strength between the CB nanoparticles and the PDMS substrate. Micro-nano structures were formed by spraying solution containing CB particles, while the SEBS reduced surface energy of the coating, thus resulting in the superhydrophobic surface. As shown in Fig. 2a, with the increase of the SEBS mass percentage, the CA of the sample decreased slightly, while the RA of the sample increased sharply. To explore the reasons for the above phenomenon, we observed microstructures of the coating surface, as shown in Fig. 2b–d. When the mass percentage of the SEBS was 25%, the CB nanoparticles were densely packed, and the surface was relatively rough. When the mass percentage of SEBS was 75%, there was almost no CB nanoparticles protruding the surface, and the surface became flat. This was because the SEBS gradually encapsulated the CB nanoparticles with the increase of the SEBS percentage, which reduced the micro-nano structures of the coating surface, and thereby increased the adhesion of the coating surface. As a result, the CA and RA differed obviously at different SEBS percentages. When the mass percentage of the SEBS was 25%, the CA of the sample was $153 \pm 2.83°$ and the RA was $8.5 \pm 1.04°$, showing low adhesion and good superhydrophobicity. In addition, the C, O, and Si elements were evenly distributed over the surface, as shown in the elemental mapping image (Fig. S1).

3.2 Performance of Flexible Strain Sensor

The above results showed that the coating was superhydrophobic with the CA greater than 150° and the RA lower than 10°. We then investigated sensing performance of the flexible strain sensor. The samples were cut into rectangular strips of 46 mm × 10 mm. The resistance of a conductor with a certain electrical conductivity was closely related to its cross-sectional area and length. Linear stretching led to a change in the conductive path, decreasing the cross-sectional area while increasing the conductive length. In addition, as the sample was stretched to a certain length, the distance between the CB nanoparticles would increase, reducing the effective connection of the conductive channels of the coating and making it less conductive. With the combination of the above two factors, the prepared superhydrophobic flexible sensor could be regarded as a strain sensor to convert a mechanical signal into a resistive signal. The resistance R of the CB-SEBS/PDMS films was measured simultaneously with a digital multimeter during stretching [32]. The experimental measurement points and fitted curves for $\Delta R/R_0$-ε are shown in Fig. 3a. $\Delta R/R_0$ increased monotonically with the tensile strain, and showed a linear relationship in the range of 0%–70%. However, the resistance had different response rates in different strain regions, which indicated that the sensor showed different sensitivities to strain. According to sensitivity Eq. (1), the gauge factor (GF) in different strain ranges can be obtained as follows [33],

$$GF = \frac{\Delta R/R_0}{\varepsilon} \tag{1}$$

where $\Delta R = R - R_0$, R_0 is the film resistance at the relaxed state [34], $\varepsilon = (L - L_0)/L_0$, L and L_0 are the film lengths at the tensile state and the relaxed state, respectively.

The gauge factor is 5.4 in the strain region of $0\% < \varepsilon < 10\%$, 7.3 in the strain region of $10\% < \varepsilon < 40\%$, and 5.8 in the strain region of $40\% < \varepsilon < 70\%$. All three fitted curves showed a good linear relationship between the two parameters, normalized resistance $\Delta R/R_0$ and ε (R^2 of 0.9877, 0.9940, and 0.9950 respectively). The GF varied with the strain range. In the small strain range of 0%–10%, the distance between the conductive particles became larger due to the stretching, resulting in a corresponding change in resistance; however, the conductive network was not significantly disrupted, therefore, the change in resistance was not very significant and the GF was small. By contrast, in the strain range of 10%–40%, as the tensile deformation continued increasing, the conductive network was further disrupted and the distance between the conductive particles increased, severely decreasing the effective conductive path; as a result, the resistance increased obviously, and the GF value at this point was larger than that in the small strain of 0%–10%. When the strain was 40%–70%, the GF value was smaller, because the coating was more flexible due to the addition of SEBS, and did not deform as much as the substrate, so the conductive network connection was not more seriously damaged by the further increase in strain. Shown in Fig. 3b is the strain-sensing behavior under cyclic tensile testing with different strains from 10% to 70%. The normalized resistance $\Delta R/R_0$ increased sharply as the maximum strain range increased from 10% to 70%, and also exhibited an accurate and repeatable signal at the different stretching-releasing strain cycles. As shown in Fig. 3c, the normalized resistance curve had a certain hysteresis in the tension and response process, but the maximum hysteresis error was only 4.8%. In addition, the sensor had a highly repeatable response under multiple cycles of loading. The change in sensor resistance from $\varepsilon = 0\%$ to $\varepsilon = 10\%$ over 100 stretch-release cycles at a stretch rate of 0.5 mm/s was shown in Fig. 3d. It could be seen that the normalized resistance $\Delta R/R_0$ maintained a relatively constant signal output, and did not change significantly during the 100 stretching-releasing cycles. The results demonstrated that the CB-SEBS/PDMS strain sensor possessed excellent repeatability at relatively small strains

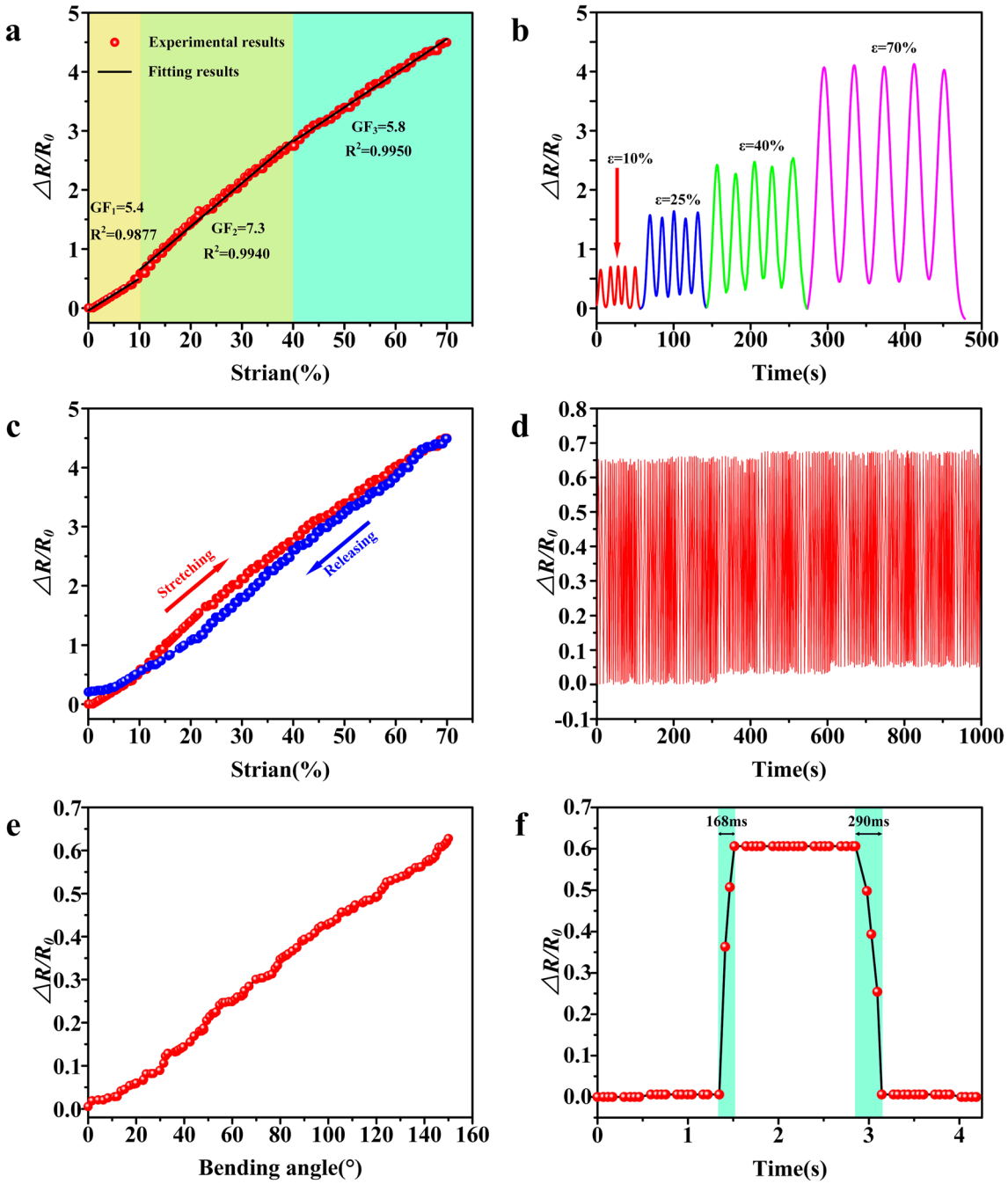

Fig. 3 **a** Experimental measurement points and fitted curves of normalized resistance versus strain ε for the CB-SEBS/PDMS strain sensors. **b** Variation of normalized resistance $\Delta R/R_0$ for the CB-SEBS/PDMS strain sensors during five cycles of stretching-releasing at strains ranging from 10% to 70%. **c** Variation of $\Delta R/R_0$ for the CB-SEBS/PDMS strain sensors during one stretching-releasing. **d** Variation of normalized resistance $\Delta R/R_0$ for the CB-SEBS/PDMS strain sensors tested for 100 stretch-response cycles from $\varepsilon = 0\%$ to $\varepsilon = 10\%$ at a stretch rate of 0.5 mm/s. **e** Variation of normalized resistance $\Delta R/R_0$ for the CB-SEBS/PDMS strain sensors with bending angle. **f** Response and recovery time of the CB-SEBS/PDMS strain sensors

(0%–10%). Besides stretching, deformation from bending is also a common type of mechanical deformation. To achieve signal detection of bending deformation, the CB-SEBS/PDMS strain sensor was fitted on a silicone rod, which was fixed at one end and bent at the other. The bending of the silicone rod caused a strain on the sensor, which resulted in a change in the resistance signal. The normalized resistance of the CB-SEBS/PDMS strain sensor versus the bending angle is shown in Fig. 3e. The sensor could well detect bending deformation with a wide bending detection range of up to

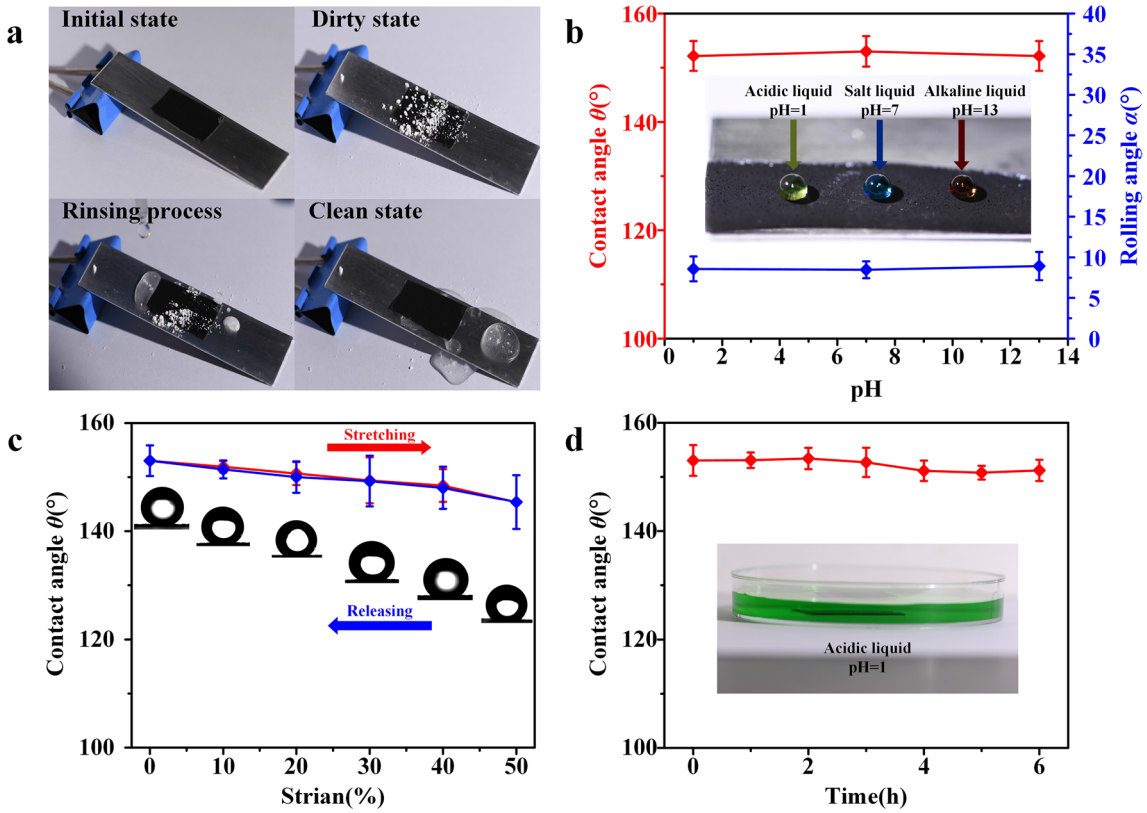

Fig. 4 **a** Self-cleaning process for contaminants on the CB-SEBS/PDMS strain sensor surface. **b** Contact angles of the CB-SEBS/PDMS strain sensor surface with droplets of different pH. **c** Contact angle of the CB-SEBS/PDMS strain sensor in the stretching-releasing process. **d** Contact angle of the CB-SEBS/PDMS strain sensor surface after being immersed in an acid solution (HCl) of pH = 1 for different times

150°. To investigate response time of the CB-SEBS/PDMS strain sensor, a tensile-release test with a strain of 10% was performed on the sensor, as shown in Fig. 3f. The strain sensor exhibited a tensile response time of 168 ms and a recovery response time of 290 ms, possessing a fast response rate.

3.3 Self-Cleaning and Anti-Corrosion Properties

In practical applications, the CB-SEBS/PDMS strain sensor may come into contact with dust, acid, base, and other corrosive contaminants from the environment, which will lead to deterioration in the sensing performance. Therefore, it is of great significance to investigate the self-cleaning and the anti-corrosion properties of the superhydrophobic CB-SEBS/PDMS films. To test the self-cleaning performance, we placed chalk dust as the contaminant source on the CB-SEBS/PDMS film, and rinsed with water droplets. Figure 4a revealed that the water droplets could easily take away the contaminants from the surface of the CB-SEBS/PDMS film, indicating good self-cleaning performance. As shown in Fig. 4b and Fig. S2, we dropped 5 µl of the HCl aqueous solution, the NaCl aqueous solution, and NaOH aqueous solution on the CB-SEBS/PDMS film surface, respectively. In order to distinguish the three solutions of acids, bases, and salts more visually, we respectively dyed the hydrochloric acid, sodium chloride, and sodium hydroxide solutions as green, blue, and red using water dyes. All the droplets maintained good spherical shapes on the CB-SEBS/PDMS film surface with the CAs of 152.2 ± 2.77° at pH = 1, 153 ± 2.83° at pH = 7, and 151.1 ± 4.13° at pH = 13. In addition, the droplets of the HCl aqueous solution, the NaCl aqueous solution, and NaOH aqueous solution could easily roll off the CB-SEBS/PDMS film surface, which illustrated that it was difficult for the corrosive liquids to adhere to the CB-SEBS/PDMS film surface. Figure 4c shows the corresponding change in CA during one stretching-releasing. The CA of the surface decreased from 153 ± 2.83° to 145.4 ± 5.97° when the strain increased to 50% during the stretching process. As the film was released to its initial state, it returned to its original value. This phenomenon could be explained by the deformation process caused by stretching and releasing. In the unstretched state, the CB nanoparticles were densely distributed, thus hindering droplet penetration. However, with the strain increased, the distance between the

CB nanoparticles increased, thus reducing superhydrophobicity. During the releasing process, the distance between the CB nanoparticles recovered, and the film surface then retained good superhydrophobicity. To test the durability of the film against corrosion, the film was placed in an acidic solution, as shown in the inset image in Fig. 4d. It can be seen that the change of CA was very slight throughout the test. The surface of the CB-SEBS/PDMS film maintained a high CA of 151.2° after being immersed in the hydrochloric acid solution for 6 h, indicating that the sensor had excellent resistance against acid corrosion. Thus, the good self-cleaning property, the excellent resistance against acid, salt, and alkali, along with the ability to maintain superhydrophobic under certain strain, may facilitate application of the sensor.

3.4 Applications for Human Motion Detection

As described above, the CB-SEBS/PDMS film with the good tensile property, corrosion resistance, and excellent durability may have promising application prospects in the wearable strain sensor that can be used for human motion detection [35–38]. We then designed a wearable strain sensor to detect the finger bending process, and its operation was shown in Fig. 5a. The tester bended the finger from horizontal to vertical (90° bend), which caused a change in the length with the stretched CB-SEBS/PDMS film. Then, we connected a resistance meter at the ends of the sensor to convert the mechanical signals into the electrical signals. Then, the tester motion was monitored by detecting changes in the resistance of the film. As shown in Fig. 5b, the normalized resistance $\Delta R/R_0$ increased with the bending angle and reached the maximum value at the maximum bending state, and the output signal had a good repeatability under the multiple repetitions of the action. In addition, we also designed a wearable strain sensor to monitor the wrist bending. The tester bended the wrist from a horizontal to a near vertical state (80° bending), as shown in Fig. 5c. The normalized resistance $\Delta R/R_0$ also increased with the bending angle, and had excellent repeatability under various repetitions, as shown in Fig. 5d. It should be noted that the resistive response was stable during human motion detection, and the sensing curves were almost identical, showing excellent durability. It can be seen that the sensor has sufficient sensitivity to rapidly and accurately output resistance signals with the changes of human motions. From the motion signal monitoring curve, we could see that the different parts of the body would show dissimilar motion signal curves during movements. Moreover, we could also judge the movement status of different parts of the body based on the electrical signal curve. Therefore, the CB-SEBS/PDMS film can effectively monitor the movement of the human body, and is expected to be applied in the field of wearable electronics.

4 Conclusions

In conclusion, we developed a low-cost and simple method to prepare a superhydrophobic flexible strain sensor with excellent properties. The superhydrophobic flexible strain

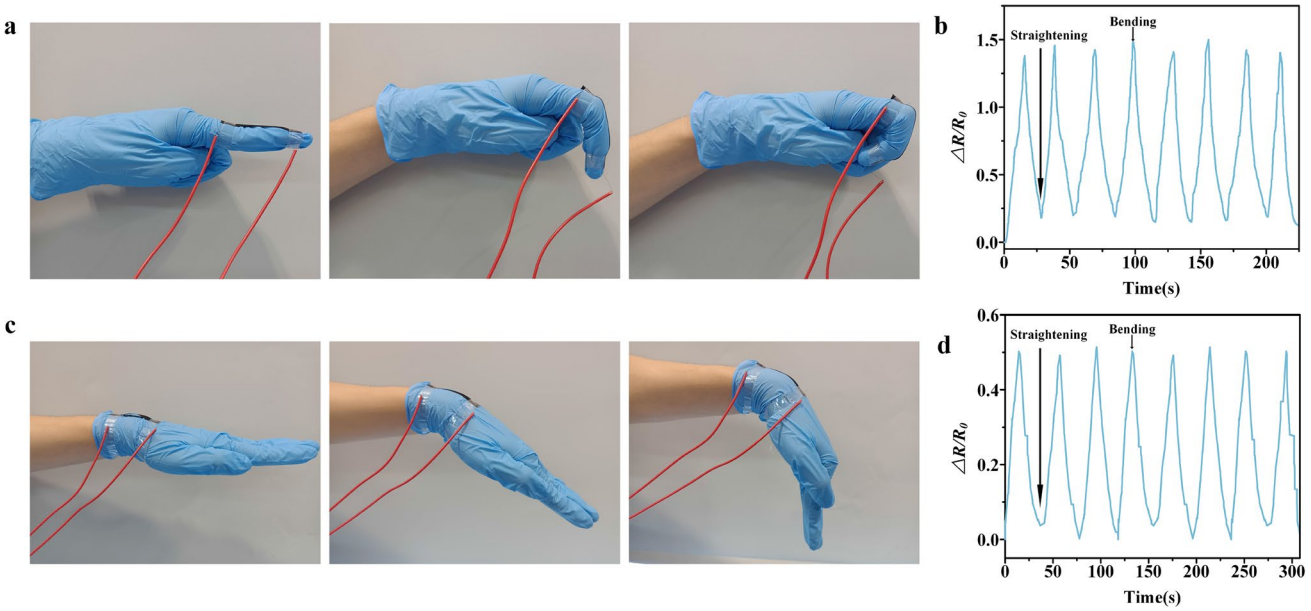

Fig. 5 **a** Schematic diagram of the finger from straightening to bending, **b** Output signal of the normalized resistance $\Delta R/R_0$ for different degrees of the finger movements of bending, **c** Schematic diagram of the wrist from straightening to bending, **d** Output signal of the normalized resistance $\Delta R/R_0$ for different degrees of the wrist movements of bending

sensor could be efficiently prepared by spraying the CB nanoparticles dispersed in the thermoplastic elastomer (SEBS) solution on the PDMS substrate. The strain sensor surface had a large water CA of $153 \pm 2.83°$ and a low RA of $8.5 \pm 1.04°$. The rolling water droplets could easily take away contaminants on the surface, indicating excellent self-cleaning property of the sensor. In addition, the superhydrophobic flexible strain sensor exhibited excellent repellency against acid, salt, and alkali liquids, which enabled the sensor to be applied in humid and corrosive conditions. The sensor also possessed good strain sensing performance, including excellent sensitivity (gauge factor (GF) of 5.4–7.35), good linearity (three linear regions), low hysteresis (hysteresis error of 4.8%), and stable response over 100 stretching-releasing cycles. Furthermore, we successfully applied the sensor to human motion detection, which could effectively detect human motion signals, such as the finger bending and the wrist bending. The fabricated superhydrophobic flexible sensor showed a broad application prospect in the field of wearable electronic devices.

Supplementary Information The online version contains supplementary material available at https://doi.org/10.1007/s41871-023-00183-9.

Acknowledgements This work was supported by National Natural Science Foundation of China (Grant No.51975092), and the Fundamental Research Funds for the Central Universities (Grant No. DUT19ZD202).

Author contributions All authors read and approved the final manuscript.

Availability of Data and Materials The author declare that all data supporting the findings of this study are available within the article.

Declaration

Conflict of Interest All authors declare that they have no competing interests.

References

1. Jo YK, Jeong S, Moon YK, Jo Y, Yoon J, Lee J (2021) Exclusive and ultrasensitive detection of formaldehyde at room temperature using a flexible and monolithic chemiresistive sensor. Nat Commun. https://doi.org/10.1038/s41467-021-25290-3
2. Adachi K, Matsukuma H, Sugawara T, Shimizu Y, Gao W, Niwa E, Sasaki Y (2019) Integration of a Cr–N thin-film displacement sensor into an XY micro-stage for closed-loop nano-positioning. Nanomanuf Metrol 2:131–139. https://doi.org/10.1007/s41871-019-00040-8
3. Liu Q, Lu Z, Liu Z, Lin P, Wang X (2022) Ballast water dynamic allocation optimization for revolving floating cranes based on a hybrid algorithm of fuzzy-particle swarm optimization with domain knowledge. J Mar Sci Eng 10:1454. https://doi.org/10.3390/jmse10101454
4. Peng X, Kong L, Chen Y, Shan Z, Qi L (2020) Design of a multi-sensor monitoring system for additive manufacturing process. Nanomanuf Metrol 3:142–150. https://doi.org/10.1007/s41871-020-00062-7
5. Xu Q, Xiao S, Gao H, Shen H (2022) The propagation of fibre–matrix interface debonding during CFRP edge milling process with the multi-teeth tool: a model analysis. Compos Part A-Appl S 160:107050. https://doi.org/10.1016/j.compositesa.2022.107050
6. Cui J, Chen J, Ni Z, Dong W, Chen M, Shi D (2022) High-sensitivity flexible sensor based on biomimetic strain-stiffening hydrogel. ACS Appl Mater Interfaces 14:47148–47156. https://doi.org/10.1021/acsami.2c15203
7. Barthlott W, Neinhuis C (1997) Purity of the sacred lotus, or escape from contamination in biological surfaces. Planta 202:1–8. https://doi.org/10.1007/s004250050096
8. Cai Y, Xu Z, Wang H, Lau KHA, Ding F, Sun J, Qin Y, Luo X (2019) A sequential process for manufacturing nature-inspired anisotropic superhydrophobic structures on AISI 316L stainless steel. Nanomanuf Metrol 2:148–159. https://doi.org/10.1007/s41871-019-00046-2
9. Chen Y, Yan D, Liu R, Lu Y, Zhao D, Deng X, Song J (2022) Green self-propelling swimmer driven by rain droplets. Nano Energy 101:107543. https://doi.org/10.1016/j.nanoen.2022.107543
10. Liu Z, Liu H, Li W, Song J (2022) Optimization of bioinspired surfaces with enhanced water transportation capacity. Chem Eng J 433:134568. https://doi.org/10.1016/j.cej.2022.134568
11. Sun Y, Wang Y, Sui X, Liang W, He L, Wang F, Yang B (2021) Biomimetic multiwalled carbon nanotube/polydimethylsiloxane nanocomposites with temperature-controlled, hydrophobic, and icephobic properties. ACS Appl Nano Mater 4:10852–10863. https://doi.org/10.1021/acsanm.1c02275
12. Wang Y, Sun Y, Xue Y, Sui X, Wang F, Liang W, Dong Q (2022) Multifunctional electro-thermal superhydrophobic shape memory film with in situ reversible wettability and anti-icing/deicing properties. Colloids Surf A 654:129960. https://doi.org/10.1016/j.colsurfa.2022.129960
13. Wang D, Sun Q, Hokkanen MJ, Zhang C, Lin F, Liu Q, Zhu S, Zhou T, Chang Q, He B et al (2020) Design of robust superhydrophobic surfaces. Nature 582:55–59. https://doi.org/10.1038/s41586-020-2331-8
14. Sun Y, Sui X, Wang Y, Liang W, Wang F (2020) Passive anti-icing and active electrothermal deicing system based on an ultraflexible carbon nanowire (CNW)/PDMS biomimetic nanocomposite with a superhydrophobic microcolumn surface. Langmuir 36:14483–14494. https://doi.org/10.1021/acs.langmuir.0c01745
15. Dai Z, Chen G, Ding S, Lin J, Li S, Xu Y, Zhou B (2021) facile formation of hierarchical textures for flexible, translucent, and durable superhydrophobic film. Adv Funct Mater 31:2008574. https://doi.org/10.1002/adfm.202008574
16. Jiang Y, Chen Y, Wang W, Yu D (2021) A wearable strain sensor based on polyurethane nanofiber membrane with silver nanowires/polyaniline electrically conductive dual-network. Colloids Surf A 629:127477. https://doi.org/10.1016/j.colsurfa.2021.127477

17. Liu K, Yang C, Zhang S, Wang Y, Zou R, Alamusi DQ, Hu N (2022) Laser direct writing of a multifunctional superhydrophobic composite strain sensor with excellent corrosion resistance and anti-icing/deicing performance. Mater Des. https://doi.org/10.1016/j.matdes.2022.110689
18. Sun F, Huang X, Wang X, Liu H, Wu Y, Du F, Zhang Y (2021) Highly transparent, adhesive, stretchable and conductive PEDOT:PSS/polyacrylamide hydrogels for flexible strain sensors. Colloids Surf A 625:126897. https://doi.org/10.1016/j.colsurfa.2021.126897
19. Xu Q, Bao Y, Wang Y, Gao H (2021) Investigation on damage reduction method by varying cutting angles in the cutting process of rectangular Nomex honeycomb core. J Manuf Process 68:1803–1813. https://doi.org/10.1016/j.jmapro.2021.07.006
20. Ding Y, Xue C, Guo X, Wang X, Jia S, An Q (2021) Fabrication of TPE/CNTs film at air/water interface for flexible and superhydrophobic wearable sensors. Chem Eng J 409:128199. https://doi.org/10.1016/j.cej.2020.128199
21. Wang J, Liu Y, Wang S, Liu X, Chen Y, Qi P, Liu X (2021) Molybdenum disulfide enhanced polyacrylamide-acrylic acid-Fe3+ ionic conductive hydrogel with high mechanical properties and anti-fatigue abilities as strain sensors. Colloids Surf A 610:125692. https://doi.org/10.1016/j.colsurfa.2020.125692
22. Tang C, Zhao X, Jia J, Wang S, Zha X, Yin B, Ke K, Bao R, Liu Z, Wang Y et al (2021) Low-entropy structured wearable film sensor with piezoresistive-piezoelectric hybrid effect for 3D mechanical signal screening. Nano Energy 90:106603. https://doi.org/10.1016/j.nanoen.2021.106603
23. Gao J, Li B, Huang X, Wang L, Lin L, Wang H, Xue H (2019) Electrically conductive and fluorine free superhydrophobic strain sensors based on SiO2/graphene-decorated electrospun nanofibers for human motion monitoring. Chem Eng J 373:298–306. https://doi.org/10.1016/j.cej.2019.05.045
24. Xu W, Yang T, Qin F, Gong D, Du Y, Dai G (2019) A sprayed graphene pattern-based flexible strain sensor with high sensitivity and fast response. Sensors-Basel 19:1077. https://doi.org/10.3390/s19051077
25. Wu Y, Yan T, Pan Z (2021) Wearable carbon-based resistive sensors for strain detection: a review. IEEE Sens J 21:4030–4043. https://doi.org/10.1109/JSEN.2020.3034453
26. Wang L, Zhu R, Li G (2020) Temperature and strain compensation for flexible sensors based on thermosensation. ACS Appl Mater Inter 12:1953–1961. https://doi.org/10.1021/acsami.9b21474
27. Zhou P, Liao Y, Li Y, Pan D, Cao W, Yang X, Zou F, Zhou L, Zhang Z, Su Z (2019) An inkjet-printed, flexible, ultra-broadband nanocomposite film sensor for in-situ acquisition of high-frequency dynamic strains. Compos A 125:105554. https://doi.org/10.1016/j.compositesa.2019.105554
28. Li L, Bai Y, Li L, Wang S, Zhang T (2017) A superhydrophobic smart coating for flexible and wearable sensing electronics. Adv Mater 29:1702517. https://doi.org/10.1002/adma.201702517
29. Ma J, Pan W, Li Y, Song J (2022) Slippery coating without loss of lubricant. Chem Eng J 444:136606. https://doi.org/10.1016/j.cej.2022.136606
30. Zhang X, Xiang D, Wu Y, Harkin-Jones E, Shen J, Ye Y, Tan W, Wang J, Wang P, Zhao C et al (2021) High-performance flexible strain sensors based on biaxially stretched conductive polymer composites with carbon nanotubes immobilized on reduced graphene oxide. Compos A 151:106665. https://doi.org/10.1016/j.compositesa.2021.106665
31. Lv S, Zhang X, Yang X, Liu Q, Liu X, Yang Z, Zhai Y (2022) Slippery surface with honeycomb structures for enhancing chemical durability of aluminum. Colloids Surf A 648:129187. https://doi.org/10.1016/j.colsurfa.2022.129187
32. Dai Z, Ding S, Lei M, Li S, Xu Y, Zhou Y, Zhou B (2021) A superhydrophobic and anti-corrosion strain sensor for robust underwater applications. J Mater Chem A 9:15282–15293. https://doi.org/10.1039/D1TA04259A
33. Jia L, Zhou C, Dai K, Yan D, Li Z (2022) Facile fabrication of highly durable superhydrophobic strain sensors for subtle human motion detection. J Mater Sci Technol 110:35–42. https://doi.org/10.1016/j.jmst.2021.08.081
34. Yao D, Wu L, Peng S, Gao X, Lu C, Yu Z, Wang X, Li C, He Y (2021) Use of Surface penetration technology to fabricate superhydrophobic multifunctional strain sensors with an ultrawide sensing range. ACS Appl Mater Inter 13:11284–11295. https://doi.org/10.1021/acsami.0c22554
35. Liu M, Hang C, Zhao X, Zhu L, Ma R, Wang J, Lu H, Zhang DW (2021) Advance on flexible pressure sensors based on metal and carbonaceous nanomaterial. Nano Energy 87:106181. https://doi.org/10.1016/j.nanoen.2021.106181
36. Yan D, Wang Y, Liu J, Zhao D, Ming P, Song J (2021) Electrochemical 3D printing of superhydrophobic pillars with conical, cylindrical, and inverted conical shapes. Colloids Surf A 625:126869. https://doi.org/10.1016/j.colsurfa.2021.126869
37. Liu J, Yan D, Zhou Y, Chen Y, Liu X, Zhao D, Liu J, Sun J (2022) Droplet motion on superhydrophobic/superhydrophilic wedge-shaped patterned surfaces with different micro-morphologies. Colloids Surf A 647:128999. https://doi.org/10.1016/j.colsurfa.2022.128999
38. Jayathilaka WADM, Qi K, Qin Y, Chinnappan A, Serrano-García W, Baskar C, Wang H, He J, Cui S, Thomas SW et al (2019) Significance of nanomaterials in wearables: a review on wearable actuators and sensors. Adv Mater 31:1805921. https://doi.org/10.1002/adma.201805921